The Astrophysical Journal Letters, 990:L57 (8pp), 2025 September 10 https://doi.org/10.3847/2041-8213/adff82

Optical Spectroscopy of the Most Compact Accreting Binary Harboring a Magnetic White Dwarf and a Hydrogen-rich Donor

Ilkham Galiullin[1], Antonio C. Rodriguez[2], Kareem El-Badry[2], Ilaria Caiazzo[2,3], Paula Szkody[4], Pranav Nagarajan[2], and Samuel Whitebook[2]
[1] Kazan Federal University, Kremlevskaya Str.18, 420008, Kazan, Russia; IlhIgaliullin@kpfu.ru
[2] Department of Astronomy, California Institute of Technology, 1200 E California Blvd, Pasadena, CA 91125, USA
[3] Institute of Science and Technology Austria, Am Campus 1, 3400, Klosterneuburg, Austria
[4] Department of Astronomy, University of Washington, 3910 15th Avenue NE, Seattle, WA 98195, USA
Received 2025 July 31; revised 2025 August 21; accepted 2025 August 25; published 2025 September 8

Abstract

Accreting white dwarfs (WDs) in close binary systems, commonly known as cataclysmic variables (CVs), with orbital periods below the canonical period minimum (≈80 minutes) are rare. Such short periods can only be reached if the donor star in the CV is either significantly evolved before initiating mass transfer to the WD or is metal-poor. We present optical photometry and spectroscopy of Gaia19bxc, a high-amplitude variable identified as a polar CV with an exceptionally short orbital period of 64.42 minutes—well below the canonical CV period minimum. High-speed photometry confirms persistent double-peaked variability consistent with cyclotron beaming, thus indicating the presence of a magnetic WD. Phase-resolved Keck/Low-Resolution Imaging Spectrometer (LRIS) spectroscopy reveals strong hydrogen and helium emission lines but no donor features, indicating the accretor is a magnetic WD and the donor is hydrogen-rich, but cold and faint. The absence of a detectable donor and the low inferred temperature ($\lesssim$3500 K) disfavor an evolved donor scenario. Instead, the short period and the system's halo-like kinematics suggest Gaia19bxc may be the first known metal-poor polar. Because metal-poor donors are more compact than solar-metallicity donors of the same mass, they can reach shorter minimum periods. Gaia19bxc is one of only a handful of known metal-poor CVs below the canonical period minimum and has the shortest period of any such magnetic system discovered to date.

Unified Astronomy Thesaurus concepts: Binary stars (154); Cataclysmic variable stars (203); White dwarf stars (1799)

1. Introduction

Binary star systems harboring a compact object are important astrophysical laboratories, serving as probes of mass transfer in magnetic and nonmagnetic environments, binary effects on stellar evolution, and in the most extreme systems, supernovae and gravitational waves. The most abundant and nearby systems, due to the initial mass function, are binaries containing a white dwarf (WD). Cataclysmic variables (CVs) are close binary systems consisting of a WD and a Roche lobe-filling main-sequence companion. In such binaries, a WD accretes matter from a donor star via the inner Lagrangian point. CVs can be magnetic systems (polars and intermediate polars, IPs) or nonmagnetic systems (novae, dwarf novae, and nova-like variables), depending on the WD's magnetic field strength (B) (B. Warner 1995). The strong magnetic field strength of a WD in polars ($B \approx$ 10–250 MG) can prevent the formation of an accretion disk, and matter falls directly onto the surface of a WD. In the case of IPs, a moderate magnetic field of a WD ($B \lesssim 1$ MG) can disrupt the formation of only the inner part of the accretion disk. In nonmagnetic CVs, the disk meets the WD surface, and a boundary layer is formed. Some CVs undergo stable or unstable hydrogen or helium burning on the surface of the WD (K. Nomoto et al. 2007; W. M. Wolf et al. 2013), resulting in observed phenomena such as nova outbursts, recurrent novae, and, in the single-degenerate scenario, Type Ia supernovae (J. Whelan & I. Iben 1973; K. Nomoto 1982). Being one of the most common classes of X-ray sources in our Galaxy, CVs are thought to significantly contribute to the Galactic ridge X-ray emission (M. Revnivtsev et al. 2006). Recently, magnetic CVs have been found to make up nearly a third of all CVs (A. F. Pala et al. 2020; A. C. Rodriguez et al. 2025b), and exotic systems featuring rapidly evolving WDs (e.g., A. C. Rodriguez et al. 2025a) and radio and X-ray pulsations (e.g., T. R. Marsh et al. 2016; I. Pelisoli et al. 2023) may shine a light on their complex evolution (e.g., M. R. Schreiber et al. 2021).

The evolution of CVs is governed by angular momentum loss, primarily through gravitational wave radiation and magnetic braking, which drives orbital shrinkage and leads to shorter orbital periods (B. Paczyński 1967). For hydrogen-dominated CVs accreting from main-sequence donors, the observed minimum orbital period is ≈82 minutes (B. T. Gänsicke et al. 2009), while theoretical models predict a shorter minimum of ≈76 minutes (C. Knigge 2006). The orbital period of a majority of CVs varies from ≈80 minutes up to 10 hr. In rare cases, CVs have orbital periods below the canonical period minimum. The donor in such a CV must be denser than a normal low-mass star at the hydrogen burning limit. This can occur if the donor has evolved significantly and formed a helium-rich core before overflowing its Roche lobe (A. V. Tutukov et al. 1985). The evolved CV donor is hotter and smaller compared to normal CV donors (e.g., K. El-Badry et al. 2021a, 2021b). Evolved CVs may evolve toward shorter orbital periods and become AM Canum Venaticorum (AM CVn) systems (e.g., P. Podsiadlowski et al. 2003; D. Belloni & M. R. Schreiber 2023; A. Sarkar et al. 2023a, 2023b). AM CVns are ultracompact binaries and have

orbital periods in the 5.4–67.8 minutes range (see e.g., J. E. Solheim 2010; G. Ramsay et al. 2018). Their optical spectra are dominated by helium emission lines, which makes them easily distinguishable from other CVs. Around 100 of the AM CVn stars are currently known (G. Ramsay et al. 2018; M. J. Green et al. 2025). Among the known AM CVn systems, only two have been suggested to host moderately magnetic WDs (10^4–10^5 G; T. J. Maccarone et al. 2024).

Alternatively, CVs can reach periods below the canonical period minimum if they form from low-metallicity ("Population II") stars, which are more compact than solar-metallicity stars of the same mass (S. B. Howell & P. Szkody 1990; R. Stehle et al. 1997). Due to lower metallicity, Population II stars might have a period minimum of 51–67 minutes (R. Stehle et al. 1997), which is shorter than for Population I CVs.

The Gaia Photometric Science Alerts Team reported Gaia19bxc[5] as a transient object on 2019 May 23 (A. Delgado et al. 2019; S. T. Hodgkin et al. 2021). T. Kato (2022) showed that Gaia19bxc exhibits high- and low-state variability, along with a 64.42 minute period in the Zwicky Transient Facility (ZTF) data. This behavior led T. Kato (2022) to suggest that Gaia19bxc was likely a magnetic CV with a strong magnetic field, known as a polar. In this Letter, we show that Gaia19bxc has both a photometric and spectroscopic 64.42 minute period, strongly suggesting that this is the orbital period of the system. Phase-resolved spectroscopy reveals that this is a H-rich (not He-rich) system as well as evidence cyclotron beaming. This suggests that Gaia19bxc is a polar and would therefore have a magnetic field strength $B \gtrsim 10$ MG. This is the first such system; of the known H-rich CVs[6] with orbital periods $P_{\rm orb} \lesssim 78$ minutes (e.g., M. J. Green et al. 2020), none have been found to host a strongly magnetic WD. We present optical observations of Gaia19bxc, including high-speed photometry with the Caltech High-speed Multi-color CAMERA (CHIMERA) on the Hale Telescope and phase-resolved spectroscopy using Keck I/Low-Resolution Imaging Spectrometer (LRIS; see Section 2) We discuss the evolutionary stage of Gaia19bxc in Section 3.

2. Data and Analysis

2.1. Archival ZTF Data and High-speed Optical Photometry with CHIMERA

The top-left panel of Figure 1 shows the long-term optical ZTF light curves (r and g filters) of Gaia19bxc. We selected the part of the long-term light curve at high state between the time of MJD = (58500, 58750) days to search for the period. We used the Lomb–Scargle periodogram to search for the periodic signal ranging from 5 minutes to 1 day. We detect only two significant peaks on the Lomb–Scargle periodogram corresponding to the best period of 64.420 ± 0.006 minutes and its harmonics (half of the best-fit period; see Figure 1, top-right panel). The error of the photometric period is estimated from using a Monte Carlo analysis, attempting to recover a significant repeating signal assuming different periods. This period is consistent with one reported by T. Kato (2022). We found no significant periods (e.g., WD spin period) aside from the best-fit period 64.42 minutes in the ZTF light curve. We also searched for the possible period in different parts of the long-term light curve but found no period besides the 64.42 minutes. The bottom-left panel of Figure 1 shows the phase-folded r-filter ZTF light curve with the period of 64.42 minutes. For obtaining orbital phases, $T_{\rm ref}$ in this Letter is arbitrarily set to 60301.001 (MJD). The light curve shows two peaks, corresponding to brightness change of 2.5 mag at phase $\phi = 0.25$ and 1.5 mag at phase $\phi = 0.75$.

We obtained high-speed photometry of Gaia19bxc on 2023 May 25 using CHIMERA (L. K. Harding et al. 2016) on the Hale 200 inch telescope. Both data in Sloan i and g filters were acquired at a 10 s cadence simultaneously, covering about 120 minutes (about 1.5 times of the orbital period of Gaia19bxc). We calibrated CHIMERA data using standard techniques. In Appendix A, we present the full high-speed photometry data. The bottom-right panel of Figure 1 shows the CHIMERA g and i filter high-speed photometry light curves of Gaia19bxc folded over the 64.42 minute orbital period. This confirms that the 64.42 minute period is the orbital period of Gaia19bxc. Similarly to archival ZTF data, CHIMERA's light curves show two peaks at approximately phases of $\phi = 0.25$ and $\phi = 0.75$. Such a behavior of the light curve is typical for polars, showing variability within a single orbital period due to cyclotron beaming. According to the two-component cyclotron model from R. K. Campbell et al. (2008), two peaks in a single orbital period of Gaia19bxc can be due to the viewing angles of the system or a complex magnetic field structure (see also J. van Roestel et al. 2025). A detailed light-curve modeling of the Gaia19bxc is beyond the scope of this Letter.

2.2. Phase-resolved Optical Spectroscopy and Doppler Tomography

We obtained a phase-resolved spectroscopy of Gaia19bxc over the photometric period on 2023 June 23 with Keck I telescope using LRIS (J. B. Oke et al. 1995). The 600/4000 grism (2 × 2 binning) was used on the blue side and the 400/8500 grism on the red side (2 × 1 binning). A 1.″0 slit was used, and the seeing during the observation was approximately 1.″2, leading to possible slit losses. Light cirrus clouds may have additionally led to a reduced throughput. We reduced the Keck I/LRIS data using standard techniques. The data were wavelength calibrated with internal lamps, flat-fielded corrected, and cleaned for cosmic rays with `lpipe`, which is a pipeline optimized for LRIS imaging and long-slit spectroscopy (D. A. Perley 2019).

The left panel of Figure 2 shows phase-resolved spectra of Gaia19bxc. Orbital phases on the left panel are obtained from $T_{\rm ref}$ as specified earlier, and T_0 in the right panel of Figure 2 represents the start of the observation. These spectra show prominent hydrogen Balmer series along with high-excitation helium (He I and He II) emission lines. We estimated the spectroscopic period of Gaia19bxc from radial velocity (RV) measurements of selected prominent hydrogen and helium emission lines (see Appendix B). The spectroscopic period of 63.0 ± 3.9 minutes is consistent with the photometric period of 64.420 ± 0.006 minutes measured from CHIMERA light curves. We interpret this as a clear sign that the two are

[5] Celestial coordinates of Gaia19bxc are R.A. = $17^{\rm h}31^{\rm m}58\overset{\rm s}{.}5$ and decl. = +27°09′36.″2 (Gaia DR3, Gaia Collaboration et al. 2023).

[6] CVs with orbital periods below the canonical minimum include V485 Cen (T. Augusteijn et al. 1993), EI Psc (or 1RXS J232953; J. R. Thorstensen et al. 2002), CSS 100603 (E. Breedt et al. 2012), CSS 120422 (P. J. Carter et al. 2013), V418 Ser (M. Kennedy et al. 2015), KSP-OT-201701a (Y. Lee et al. 2022), ZTF J1813+4251 (K. B. Burdge et al. 2022), and KSP-OT-201712a (Y. Lee et al. 2024). The extended list can be found in M. J. Green et al. (2025).

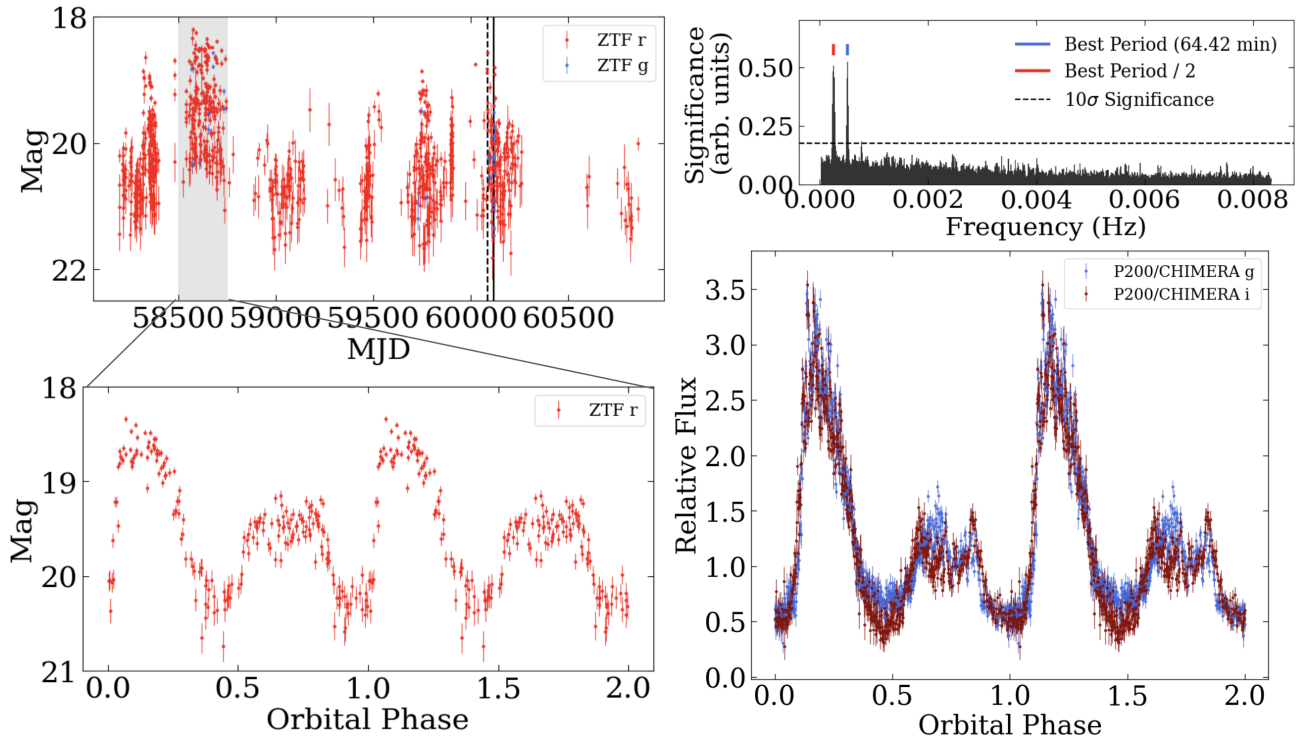

Figure 1. Archival ZTF photometry data and follow-up high-speed photometry of Gaia19bxc with CHIMERA. Upper left: the 6 yr-long ZTF light curve shows high- and low-state changes typically seen in magnetic CVs. The dashed line indicates when CHIMERA photometry was acquired, and the solid line indicates Keck I/LRIS spectroscopy. Lower left: a phase-folded ZTF light curve. A clear period is identified (64.42 minutes) while the system is in a high state. Upper right: the Lomb–Scargle periodogram of the ZTF data shows no significant periods (e.g., WD spin period) aside from 64.42 minutes. Lower right: a phase-folded CHIMERA light curve in g, i filters. Multiband high-speed (10 s) photometry confirms the double-peaked nature of the light curve from cyclotron emission and reveals no eclipses of the accreting WD.

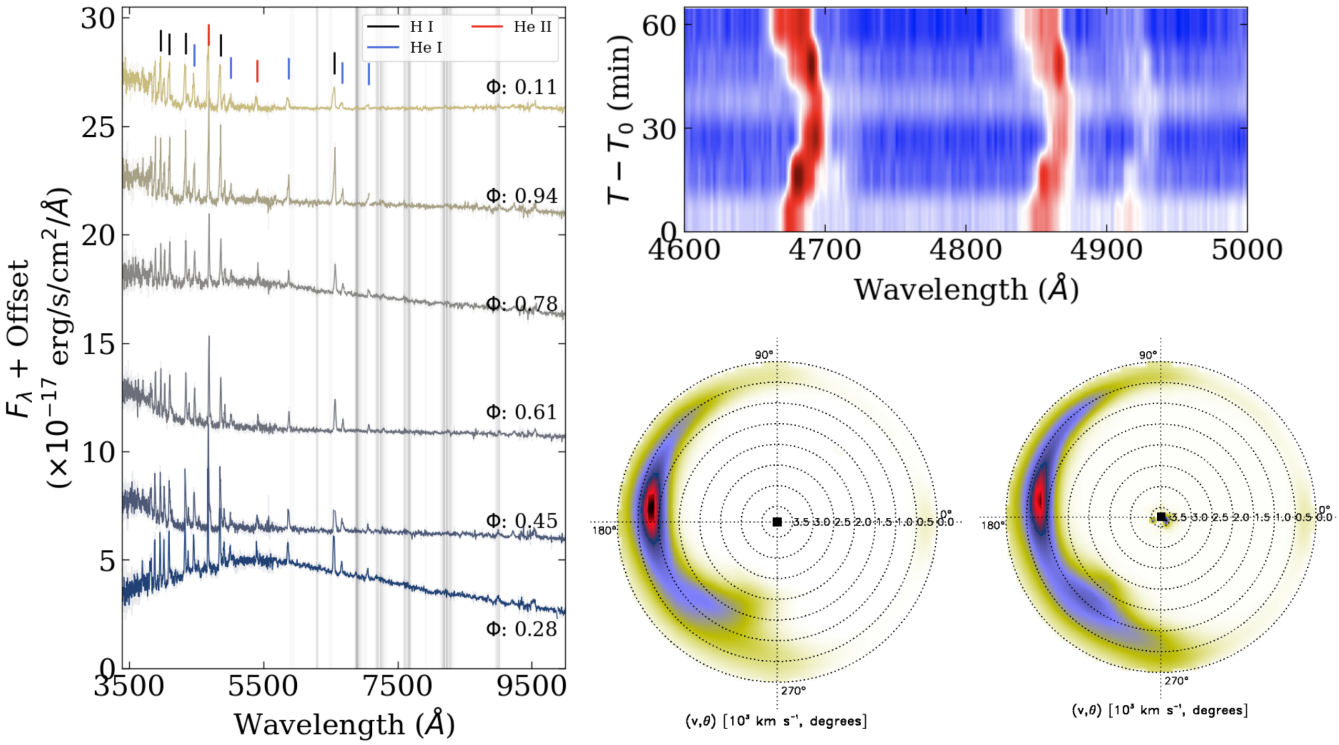

Figure 2. Left: Keck I/LRIS phase-resolved spectroscopy of Gaia19bxc. The corresponding orbital phases for each spectrum are indicated by the text. Spectra exhibit prominent hydrogen Balmer emission lines along with high-excitation helium lines (He I and He II). A broad cyclotron hump is observed at phase of $\phi = 0.28$. A small discontinuity in the spectra is caused by cosmic rays in the data. Upper right: continuum-normalized trailed spectra of the strong He II 4686 Å and Hβ emission lines and weak He I 4921 Å. Lower right: inverse Doppler tomograms of the same lines. The tomograms show no evidence of a disk structure but instead reveal a stream-like feature.

Table 1
EWs and Line Ratios of Selected Emission Lines in the Phase-averaged Spectrum of Gaia19bxc

Line (Å)	–EW (Å)
Emission lines	
Hα 6562.8	51.1 ± 6.4
Hβ 4861.3	45.9 ± 2.1
Hγ 4340.5	35.4 ± 3.2
Hδ 4101.7	32.5 ± 2.0
Hϵ 3970.1	22.6 ± 2.3
He I 4471.4	32.6 ± 4.1
He I 5015.7	30.5 ± 2.1
He I 5876.5	41.2 ± 6.3
He I 6678.2	31.3 ± 2.9
He I 7065.2	30.9 ± 2.3
He II 4685.7	46.8 ± 3.3
He I 5876.5/Hα	0.81 ± 0.16
He II 4685.7/Hβ	1.02 ± 0.09

consistent with the orbital period of the system, confirming its nature well below the CV period minimum.

We clearly observe a broad, single cyclotron hump covering effectively all optical wavelengths in the spectrum at phase of $\phi = 0.28$, indicating the presence of a magnetic WD in the system. Based on similar characteristics seen in other polars, this implies that Gaia19bxc would have a magnetic field strength $B \gtrsim 10$ MG, though the nondetection of individual cyclotron humps prevents a more precise constraint on the magnetic field. The emission lines in the phase-resolved spectra are single-peaked, suggesting that the accretion of donor matter occurs via a stream directly onto the poles of the WD. We do not detect metal absorption lines from the donor's atmosphere or emission lines from the irradiated face of the donor. The absence of the donor's signature in the optical spectra indicates that it is a cold, late-type star. Table 1 shows the equivalent widths (EWs) of the selected emission lines computed from the phase-average Keck I/LRIS spectrum. We detect strong high-excitation He II line, yielding a line ratio of He II/H$_\beta$ = 1.02 ± 0.09. Such a line ratio is commonly seen in magnetic CVs, specifically in polars (e.g., A. D. Silber 1992).

The top-right panel of Figure 2 shows the trailed, continuum-normalized Keck I/LRIS spectra for the He II 4686 Å and Hβ emission lines. Over the entire 64.42 minute orbital period, the RV shifts of these lines are about 500 km s^{-1}, typical for polars. We also present Doppler tomograms for the He II 4686 Å and Hβ lines, which map line shifts and strengths into velocity as a function of orbital phase (e.g., T. R. Marsh & K. Horne 1988). We used the `doptomog`[7] code developed by E. J. Kotze et al. (2015) to construct Doppler tomograms shown here. The "inverse"[8] Doppler tomograms for these emission lines reveal no disk structure. Instead, a stream-like feature is observed, resembling those commonly seen in polars (see Figure 2, bottom-right panel).

[7] https://www.saao.ac.za/~ejk/doptomog/main.html

[8] This refers to the manner in which velocities are shown in polar coordinates: "inverse" Doppler tomograms show higher velocities inside, lower velocities outside.

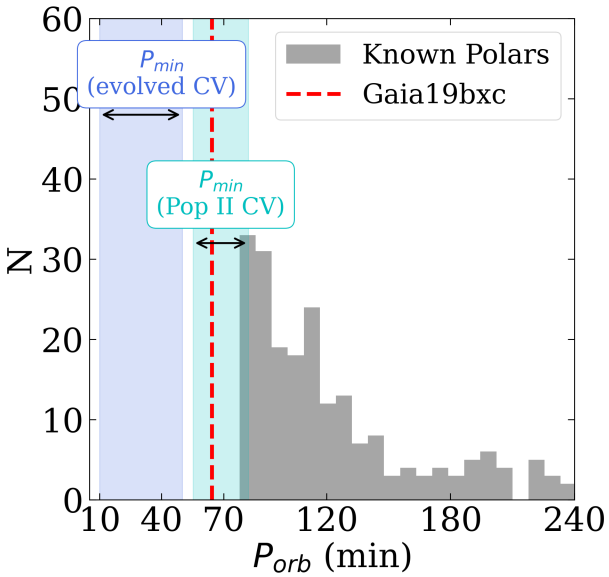

Figure 3. The period distribution of known polars from H. Ritter & U. Kolb (2003; gray). The orbital period of Gaia19bxc, with its 64.42 minute period. is marked by the red vertical line, showing that Gaia19bxc is the most compact polar known to date. The cyan region indicates the predicted $P_{\rm min}$ range (51–78 minutes) for Population II (metal-poor) CVs (see Table 2 of R. Stehle et al. 1997). The blue region represents the predicted $P_{\rm min}$ range (10–50 minutes) for evolved CVs from the MESA models of K. El-Badry et al. (2021a). Since both evolutionary paths lead to period minima below the orbital period of Gaia19bxc, a clear detection and characterization of the donor of Gaia19bxc would be crucial to distinguish between these two scenarios.

3. Discussion and Conclusion

High-speed photometry and phase-resolved spectroscopy indicate that Gaia19bxc is a polar with an orbital period of 64.42 minutes. Such an orbital period is well below the canonical period minimum ($P_{\rm min}$) for CVs (≈76 minutes, C. Knigge 2006; ≈82 minutes, B. T. Gänsicke et al. 2009), suggesting that Gaia19bxc is in a unique evolutionary stage. In Figure 3, we show that the orbital period of Gaia19bxc, while not above the $P_{\rm min}$ for typical CVs, is above that of either Population II CVs or evolved CVs. Below, we discuss three possibilities for Gaia19bxc being (a) an AM CVn, (b) an evolved CV, or (c) a Population II CV.

(a) *AM CVn system.* Gaia19bxc displays a distinctive spectroscopic signature, with optical spectra revealing both helium and hydrogen emission lines of comparable strength. Due to its ultracompact nature, one may have classified it as an AM CVn had spectroscopy not been acquired; here, we showed that this scenario is incorrect.

(b) *Evolved CV.* CVs can reach short orbital periods (below the canonical period minimum) if their donors have exhausted a significant fraction of the hydrogen in cores before filling the Roche lobe (A. V. Tutukov et al. 1985). The donor of such CVs is significantly evolved, smaller, and hotter, compared to normal CVs. Only around a dozen of CVs with orbital periods below the canonical minimum are known, likely harboring evolved donors (see footnote 6). These systems exhibit a relatively high helium-to-hydrogen line ratio, He I 5876.5/H$\alpha \lesssim 1$, comparable to Gaia19bxc, which has He I 5876.5/Hα = 0.81 (see Table 1). According to the MESA binary models for CVs with evolved donors (K. El-Badry et al. 2021a, 2021b), the donor in Gaia19bxc should be hot, with a temperature $\gtrsim$4000 K. Gaia19bxc may evolve toward a shorter orbital period via the

"evolved CV" channel, potentially becoming a magnetic AM CVn system. However, we find no evidence of a hot donor in the phase-resolved spectra of Gaia19bxc, which suggests that the donor is cooler than expected for an evolved CV (see Appendix C for more details).

(c) *Population II (metal-poor) CV.* Population II CVs represent old CVs with low-metallicity donors, formed during the early phases of Galactic evolution (S. B. Howell & P. Szkody 1990; R. Stehle et al. 1997). These CVs are predominantly located in the Galactic halo, which is metal-poor. Due to the low metallicity of their donors, Population II CVs exhibit shorter evolutionary timescales, and their period minimum varies from 51 to 59 minutes for metallicities of $Z = 10^{-5}$–10^{-3} (see Table 2 of R. Stehle et al. 1997). Being a member of the Galactic halo, Population II CVs exhibit high space velocities and proper motions. We compare the kinematic properties of Gaia19bxc to those of a known Population II CV, SDSS J150722.30+523039.8 (SDSS J15072; J. Patterson et al. 2008; H. Uthas et al. 2011). According to the Gaia DR3 catalog, SDSS J15072 is located at Galactic coordinates $(l, b) = (87.^{\circ}38, 54.^{\circ}19)$, and it shows a high proper motion of 154.84 mas yr^{-1} and a transverse velocity of approximately $\approx$156 km s^{-1}. In comparison, Gaia19bxc is located at Galactic coordinates $(l, b) = (50.^{\circ}72, 28.^{\circ}50)$, and it exhibits a high proper motion of 9.62 mas yr^{-1} with a transverse velocity of approximately $\approx$91 km s^{-1} (assuming a distance of 2 kpc; see Appendix C). These kinematic properties of Gaia19bxc are comparable to those of Population II CVs. With an orbital period of 64.42 minutes, Gaia19bxc might be a prebounce system or a period bouncer[9] of Population II CVs.

In summary, Gaia19bxc, with an orbital period of 64.42 minutes, is the first polar below the canonical period minimum of CVs. We found no evidence of a donor in the phase-resolved spectra, such as absorption lines originating from the donor's atmosphere or emission lines arising from the irradiated surface of the donor. This suggests that the donor of Gaia19bxc is cold. If Gaia19bxc were an evolved CV, the donor should be a hot, and we would expect to observe its signatures in optical spectra. Based on the discussion above, we favor the interpretation that Gaia19bxc is a Population II CV rather than an evolved CV. Our understanding of such systems is crucial since Gaia19bxc is at the faintest end ($\approx$20–21 mag) of what current photometric surveys such as ZTF can detect. In the coming years, the Rubin Observatory Legacy Survey of Space and Time (Z. Ivezic et al. 2019), reaching 23–24 mag, is bound to discover dozens more of these intrinsically faint systems, therefore increasing our understanding of magnetic field generation and evolution in close binary stars.

Acknowledgments

Based on observations obtained with the Samuel Oschin Telescope 48 inch and the 60 inch Telescope at the Palomar Observatory as part of the Zwicky Transient Facility project. ZTF is supported by the National Science Foundation under grants No. AST-1440341 and AST-2034437 and a collaboration including current partners Caltech, IPAC, the Weizmann Institute of Science, the Oskar Klein Center at Stockholm University, the University of Maryland, Deutsches Elektronen-Synchrotron and Humboldt University, the TANGO Consortium of Taiwan, the University of Wisconsin at Milwaukee, Trinity College Dublin, Lawrence Livermore National Laboratories, IN2P3, University of Warwick, Ruhr University Bochum, Northwestern University and former partners the University of Washington, Los Alamos National Laboratories, and Lawrence Berkeley National Laboratories. Operations are conducted by COO, IPAC, and UW. This work has made use of data from the European Space Agency (ESA) mission Gaia (https://www.cosmos.esa.int/gaia), processed by the Gaia Data Processing and Analysis Consortium (DPAC; https://www.cosmos.esa.int/web/gaia/dpac/consortium). Funding for the DPAC has been provided by national institutions, in particular the institutions participating in the Gaia Multilateral Agreement. Some of the data presented herein were obtained at Keck Observatory, which is a private 501(c)3 nonprofit organization operated as a scientific partnership among the California Institute of Technology, the University of California, and the National Aeronautics and Space Administration. The Observatory was made possible by the generous financial support of the W. M. Keck Foundation. We wish to recognize and acknowledge the very significant cultural role and reverence that the summit of Maunakea has always had within the Native Hawaiian community. We are most fortunate to have had the opportunity to conduct observations from this mountain. We are grateful to the staff of the Palomar and Keck Observatories for their work in helping us carry out our observations.

I.G. acknowledges support from Kazan Federal University. A. C.R. acknowledges support from the National Science Foundation via an NSF Graduate Research Fellowship. We thank the anonymous referee for useful comments and suggestions, which contributed to the improvement of this manuscript.

Appendix A
Full CHIMERA High-speed Photometry Light Curves

We calibrated CHIMERA data using standard techniques in the PyCHIMERA pipeline (bias-subtraction, flat-field correction). Aperture photometry was performed with the ULTRACAM pipeline (V. S. Dhillon et al. 2007). Relative fluxes were computed by dividing the target fluxes by those of a standard star. Figure 4 shows continuous CHIMERA light curves in g, i, and r filters covering the entire orbital period of Gaia19bxc. Approximately 90 minutes of observations with CHIMERA were obtained on 2022 August 22 (r filter) and 120 minutes on 2023 May 25 (g, i filters). The light curves were shifted to align the same phase at the starting point. The orbital period of 64.42 minutes for Gaia19bxc is confirmed with these data. The light curves in the g and i filters display a double-peaked structure at phases $\phi \approx 0.25$ and $\phi \approx 0.75$ (see Figure 1). The r-filter light curve shows a plateau at $\phi \approx 0.75$ (or $(T - T_0) \approx 50$ minutes in Figure 4) followed by a continued rise in brightness up to phase of $\phi \approx 0.8$ (or $(T - T_0) \approx 55$ minutes in Figure 4). Such differences in the light curve shapes suggest contributions from cyclotron emission.

[9] Period bouncers are CVs whose orbital periods have passed the period minimum during their evolution and are now increasing toward longer periods.

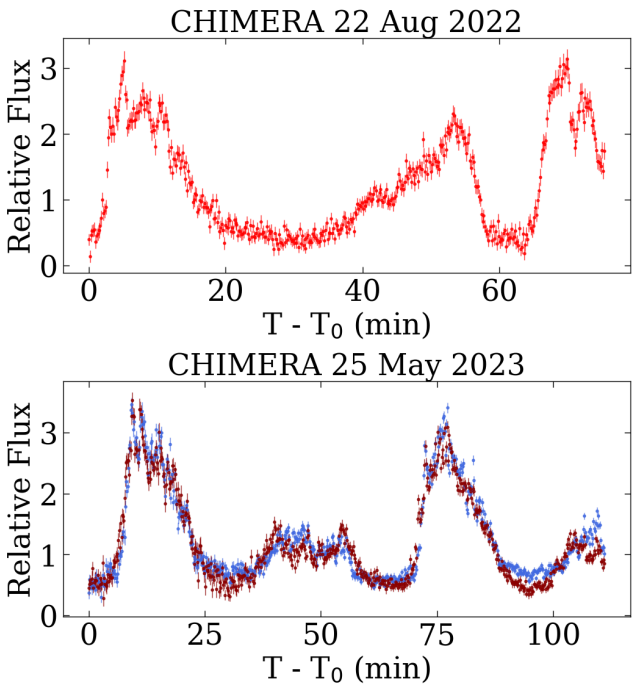

Figure 4. Full CHIMERA high-speed photometry light curves in *g*, *i*, and *r* filters covering the entire orbital period of Gaia19bxc: 2022 August 22 (*r* filter, top panel) and 2023 May 25 (*g* and *i* filters, bottom panel; blue and dark red, respectively). The orbital period of 64.42 minutes for Gaia19bxc is confirmed, which is below the period minimum for CVs.

Appendix B
RV and Spectroscopic Period Determination

We used prominent hydrogen (Hβ, Hγ) and helium (He II 4686 Å) emission lines to estimate the period of Gaia19bxc from spectroscopy alone. We fitted single-peaked Gaussian profiles to those emission lines in each phase-resolved spectrum and derived RV measurements and errors from the central wavelength of the Gaussians and error of the mean, respectively. Assuming a circular, Keplerian orbit, we used a sinusoidal function of the form

$$\mathrm{RV} = K \sin\left(\frac{2\pi(T - T_0)}{P}\right) + \gamma, \tag{B1}$$

where K is the semiamplitude of the emission line, γ is the systemic velocity, and P is the spectroscopic period. We used a Markov Chain Monte Carlo (MCMC) Bayesian parameter exploration (W. K. Hastings 1970) to generate posterior distributions of all parameters and their errors. The MCMC was performed using the *emcee* package (D. Foreman-Mackey et al. 2013) with 15,000 runs and 12 walkers, with the first half used as the burn-in period. Uniform priors were used for all parameters, where K was allowed to range between 0 and 800 km s^{-1}, γ between -500 and 500 km s^{-1}, and P between 40 and 100 minutes. Figure 5 shows the RV curves for all emission lines. By taking the weighted mean, we determined the spectroscopic period of Gaia19bxc to be 63.0 $\pm$ 3.9 minutes. This spectroscopic period is consistent with the photometric orbital period derived from CHIMERA data, the latter of which is measured to a much greater precision.

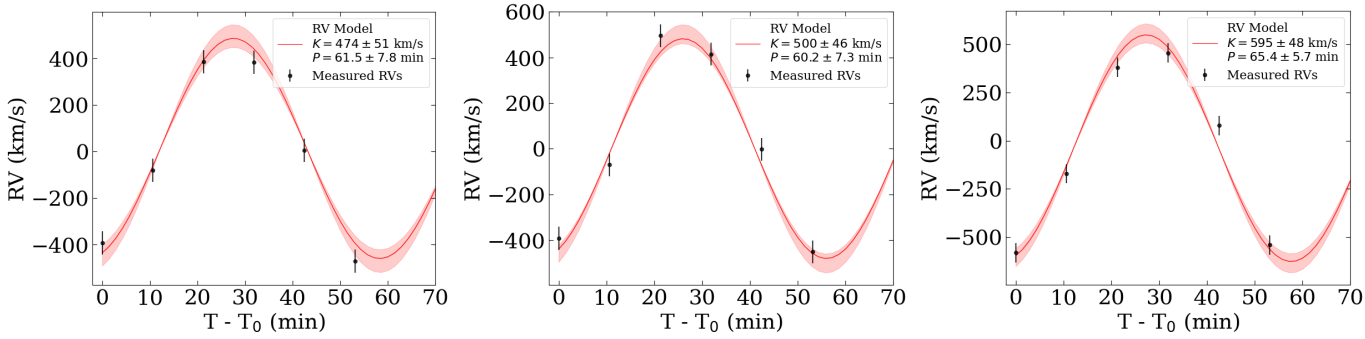

Figure 5. RV measurements (black points) of prominent hydrogen (Hβ, Hγ) and helium (He II 4686 Å) emission lines, from left to right. Solid red lines represent the RV model constructed from the median parameters of the MCMC parameter exploration. Shaded red regions indicate models constructed from the 1σ uncertainties. The mean spectroscopic period derived from their weighted average is 63.0 $\pm$ 3.9 minutes, which is consistent with the photometric period (64.42 minutes). We interpret this as the orbital period, which confirms the polar nature of the source.

Appendix C
Spectral Energy Distribution Constraints on Donor Temperature: An Unlikely Evolved Donor Scenario

We constructed the observed spectral energy distribution (SED) of Gaia19bxc based on photometric data from the Galaxy Evolution Explorer (GALEX; D. C. Martin et al. 2005), ZTF, and CatWISE catalog (P. R. M. Eisenhardt et al. 2020). No archival near-infrared photometry, X-ray, or radio detections are available for Gaia19bxc in the literature. Gaia19bxc does not have a well-constrained distance since it has a Gaia DR3 parallax of $\pi = 0.57 \pm 0.77$ mas. While the geometric distance from C. A. L. Bailer-Jones et al. (2021) is $d = 2009^{+832}_{-960}$ pc, this value should be used with caution since the parallax error exceeds the parallax measurement itself. For further analysis we adopted the fiducial distance of 2 kpc. We adopted an extinction of $A_v = 0.2$, obtained from the Bayestar19 dust map of G. M. Green et al. (2019).

The left panel of Figure 6 shows the observed SED of Gaia19bxc. The photometric data on the SED are stochastically distributed, indicating that the data are dominated by cyclotron emission at different phases of Gaia19bxc. Direct SED modeling requires the consideration of a cyclotron emission model along with WD and donor atmosphere models. We constrained the donor temperature under the assumption that all emission originates from the WD and the donor. The donor star effective temperature is specified (see Figure 6), interpolating through BT-NextGen library of theoretical stellar atmospheres (F. Allard et al. 2011), assuming solar metallicity and $\log g = 5.0$. The stellar atmosphere is multiplied by $(R/d)^2$ to obtain a flux as viewed from Earth. The same process is used for the WD, taking the theoretical (DA; H-rich) WD atmospheres of (D. Koester 2010) and assuming $\log g = 8.0$. In the WD case, $T_{WD} = 14{,}000$ K is assumed, which is typical of WDs in CVs near the fiducial period minimum, and the typical CV WD mass of $0.8 M_\odot$ is adopted A. F. Pala et al. (2022).

Adopting the fiducial distance of 2 kpc, the donor has an upper limit of $T_{\rm eff} \lesssim 3500$ K. Such a donor model fits only the ZTF r-filter flux and underestimates the Wide-field Infrared Survey Explorer (WISE) and other optical photometric data (see Figure 6, left panel). This discrepancy can be explained by the significant contribution of cyclotron emission. Conversely, a donor model with $T_{\rm eff} \approx 5000$ K fits the WISE and most of the ZTF photometric data but overestimates the ZTF r-filter flux at the light-curve minimum. A donor with $T_{\rm eff} \approx 5000$ K should be visible in optical spectra and contribute significantly to the r-filter flux. Since we do not observe donor features in the optical spectra, a donor with $T_{\rm eff} \approx 5000$ K can be ruled out. A WISE $(W_1 - W_2) \approx 1.0$ color of Gaia19bxc alone also implies an effective temperature of the donor of $T_{\rm eff} \sim 1500$ K (N. Skrzypek et al. 2015, see Table 1), assuming that only the donor radiates in the infrared.

The right panel of Figure 6 shows the donor effective temperature versus orbital period plane, along with MESA binary models for CVs with evolved donors from K. El-Badry et al. (2021a, 2021b). Models with initial orbital periods of $P_{\rm init} = 2.20$ and $P_{\rm init} = 2.46$ days correspond to initially detached WD plus main-sequence binaries. For typical CVs, the initial period is $P_{\rm init} = 1.00$ day. Binaries with initial periods of $P_{\rm init} \gtrsim 2.20$ days behave differently compared to typical CVs. The donor in such systems will evolve before filling its Roche lobe. Such CVs have an evolved donor with effective temperatures of $\gtrsim$4000 K (for models with $P_{\rm init} \gtrsim 2.2$ day). At the end of their evolution, they become AM CVn systems via the "evolved CV" channel. The upper

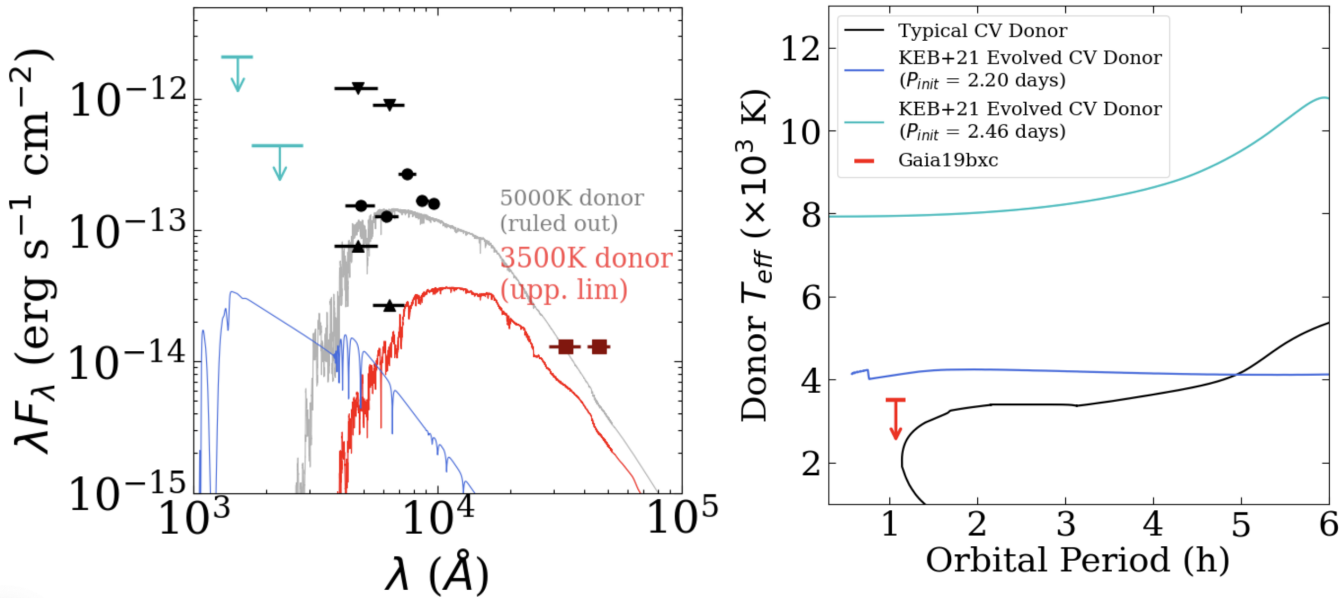

Figure 6. Left: observed SED of Gaia19bxc. Photometric data from GALEX (UV, cyan), PanSTARRS PS1 (optical; black circles), ZTF (optical; black squares), and CatWISE (mid-infrared; dark red) are shown. The ZTF data at the light-curve minimum (upward triangles) and maximum (downward triangles) are indicated in the same bandpass but with different fluxes. The blue curve represents a WD model atmosphere with $T_{\rm eff} \approx 15{,}000$ K. Adopting a fiducial distance of 2 kpc, the donor has an upper effective temperature limit of $T_{\rm eff} \lesssim 3500$ K, based on the ZTF point at light-curve minimum. A hotter donor with an effective temperature of $T_{\rm eff} \approx 5000$ K would overestimate the ZTF r-filter flux (at minimum) and should be detectable in phase-resolved spectra; however, such a donor is ruled out based on current observations. Right: donor effective temperature vs. orbital period plane. MESA binary models for evolved CV donors with initial periods $P_{\rm init} = 2.20$ (blue) and $P_{\rm init} = 2.46$ days (cyan) are adopted from K. El-Badry et al. (2021a, 2021b). A model with $P_{\rm init} = 1.00$ days (black) represents typical CVs with unevolved donors. The donor effective temperature of $T_{\rm eff} \lesssim 3500$ K places Gaia19bxc below evolved CV models (red).

limit on the donor temperature ($T_{\rm eff} \lesssim 3500$ K) places Gaia19bxc below the evolved CV models.

We note that we used a simplified approach to constrain the donor temperature of Gaia19bxc. A more precise analysis would require including cyclotron emission in the SED modeling. Gaia19bxc does not have a well-constrained distance, which further complicates the analysis. In our data, we do not detect any emission or absorption lines from the donor itself in the optical spectra. Future infrared spectroscopy of the donor is necessary to precisely determine its effective temperature and metallicity.

ORCID iDs

Ilkham Galiullin https://orcid.org/0000-0001-5778-2355
Antonio C. Rodriguez https://orcid.org/0000-0003-4189-9668
Kareem El-Badry https://orcid.org/0000-0002-6871-1752
Ilaria Caiazzo https://orcid.org/0000-0002-4770-5388
Paula Szkody https://orcid.org/0000-0003-4373-7777
Pranav Nagarajan https://orcid.org/0000-0002-1386-0603
Samuel Whitebook https://orcid.org/0000-0002-6836-181X

References

Allard, F., Homeier, D., & Freytag, B. 2011, in ASP Conf. Ser. 448, 16th Cambridge Workshop on Cool Stars, Stellar Systems, and the Sun, ed. C. Johns-Krull, M. K. Browning, & A. A. West (San Francisco, CA: ASP), 91
Augusteijn, T., van Kerkwijk, M. H., & van Paradijs, J. 1993, A&A, 267, L55
Bailer-Jones, C. A. L., Rybizki, J., Fouesneau, M., Demleitner, M., & Andrae, R. 2021, AJ, 161, 147
Belloni, D., & Schreiber, M. R. 2023, A&A, 678, A34
Breedt, E., Gänsicke, B. T., Marsh, T. R., et al. 2012, MNRAS, 425, 2548
Burdge, K. B., El-Badry, K., Marsh, T. R., et al. 2022, Natur, 610, 467
Campbell, R. K., Harrison, T. E., Schwope, A. D., & Howell, S. B. 2008, ApJ, 672, 531
Carter, P. J., Steeghs, D., de Miguel, E., et al. 2013, MNRAS, 431, 372
Delgado, A., Harrison, D., Hodgkin, S., et al. 2019, TNSTR, 2019, 1
Dhillon, V. S., Marsh, T. R., Stevenson, M. J., et al. 2007, MNRAS, 378, 825
Eisenhardt, P. R. M., Marocco, F., Fowler, J. W., et al. 2020, ApJS, 247, 69
El-Badry, K., Rix, H.-W., Quataert, E., Kupfer, T., & Shen, K. J. 2021a, MNRAS, 508, 4106
El-Badry, K., Quataert, E., Rix, H.-W., et al. 2021b, MNRAS, 505, 2051
Foreman-Mackey, D., Hogg, D. W., Lang, D., & Goodman, J. 2013, PASP, 125, 306
Gaia Collaboration, Vallenari, A., Brown, A. G. A., et al. 2023, A&A, 674, A1
Gänsicke, B. T., Dillon, M., Southworth, J., et al. 2009, MNRAS, 397, 2170
Green, M. J., Marsh, T. R., Carter, P. J., et al. 2020, MNRAS, 496, 1243
Green, G. M., Schlafly, E., Zucker, C., Speagle, J. S., & Finkbeiner, D. 2019, ApJ, 887, 93
Green, M. J., van Roestel, J., & Wong, T. L. S. 2025, arXiv:2505.10535
Harding, L. K., Hallinan, G., Milburn, J., et al. 2016, MNRAS, 457, 3036
Hastings, W. K. 1970, Bimka, 57, 97
Hodgkin, S. T., Harrison, D. L., Breedt, E., et al. 2021, A&A, 652, A76
Howell, S. B., & Szkody, P. 1990, ApJ, 356, 623
Ivezic, Z., Kahn, S. M., Tyson, J. A., et al. 2019, ApJ, 873, 111
Kato, T. 2022, arXiv:2204.04603
Kennedy, M., Garnavich, P., Callanan, P., et al. 2015, ApJ, 815, 131
Knigge, C. 2006, MNRAS, 373, 484
Koester, D. 2010, MmSAI, 81, 921
Kotze, E. J., Potter, S. B., & McBride, V. A. 2015, A&A, 579, A77
Lee, Y., Kim, S. C., Moon, D.-S., et al. 2022, ApJL, 925, L22
Lee, Y., Moon, D.-S., Kim, S. C., Park, H. S., & Ni, Y. Q. 2024, ApJ, 964, 186
Maccarone, T. J., Kupfer, T., Najera Casarrubias, E., et al. 2024, MNRAS, 529, L28
Marsh, T. R., Gänsicke, B. T., Hümmerich, S., et al. 2016, Natur, 537, 374
Marsh, T. R., & Horne, K. 1988, MNRAS, 235, 269
Martin, D. C., Fanson, J., Schiminovich, D., et al. 2005, ApJL, 619, L1
Nomoto, K. 1982, ApJ, 253, 798
Nomoto, K., Saio, H., Kato, M., & Hachisu, I. 2007, ApJ, 663, 1269
Oke, J. B., Cohen, J. G., Carr, M., et al. 1995, PASP, 107, 375
Paczyński, B. 1967, AcA, 17, 287
Pala, A. F., Gänsicke, B. T., Breedt, E., et al. 2020, MNRAS, 494, 3799
Pala, A. F., Gänsicke, B. T., Belloni, D., et al. 2022, MNRAS, 510, 6110
Patterson, J., Thorstensen, J. R., & Knigge, C. 2008, PASP, 120, 510
Pelisoli, I., Marsh, T. R., Buckley, D. A. H., et al. 2023, NatAs, 7, 931
Perley, D. A. 2019, PASP, 131, 084503
Podsiadlowski, P., Han, Z., & Rappaport, S. 2003, MNRAS, 340, 1214
Ramsay, G., Green, M. J., Marsh, T. R., et al. 2018, A&A, 620, A141
Revnivtsev, M., Sazonov, S., Gilfanov, M., Churazov, E., & Sunyaev, R. 2006, A&A, 452, 169
Ritter, H., & Kolb, U. 2003, A&A, 404, 301
Rodriguez, A. C., El-Badry, K., Hakala, P., et al. 2025a, PASP, 137, 024202
Rodriguez, A. C., El-Badry, K., Suleimanov, V., et al. 2025b, PASP, 137, 014201
Sarkar, A., Ge, H., & Tout, C. A. 2023a, MNRAS, 519, 2567
Sarkar, A., Ge, H., & Tout, C. A. 2023b, MNRAS, 520, 3187
Schreiber, M. R., Belloni, D., Gänsicke, B. T., Parsons, S. G., & Zorotovic, M. 2021, NatAs, 5, 648
Silber, A. D. 1992, PhD thesis, Massachusetts Institute of Technology
Skrzypek, N., Warren, S. J., Faherty, J. K., et al. 2015, A&A, 574, A78
Solheim, J. E. 2010, PASP, 122, 1133
Stehle, R., Kolb, U., & Ritter, H. 1997, A&A, 320, 136
Thorstensen, J. R., Fenton, W. H., Patterson, J. O., et al. 2002, ApJL, 567, L49
Tutukov, A. V., Fedorova, A. V., Ergma, E. V., & Yungelson, L. R. 1985, SvAL, 11, 52
Uthas, H., Knigge, C., Long, K. S., Patterson, J., & Thorstensen, J. 2011, MNRAS, 414, L85
van Roestel, J., Rodriguez, A. C., Szkody, P., et al. 2025, A&A, 696, A242
Warner, B. 1995, Cataclysmic Variable Stars, 28 (Cambridge: Cambridge Univ. Press)
Whelan, J., & Iben, I., Jr. 1973, ApJ, 186, 1007
Wolf, W. M., Bildsten, L., Brooks, J., & Paxton, B. 2013, ApJ, 777, 136